Guided terahertz pulse reflectometry with double photoconductive antenna

Mingming Pan, Quentin Cassar, Frederic Fauquet, Georges Humbert, Patrick Mounaix, Jean-Paul Guillet

Guided Terahertz Pulse Reflectometry with Double Photoconductive Antenna

Mingming Pan[a], Quentin Cassar[a], Frédéric Fauquet[a], Georges Humbert[b], Patrick Mounaix[a], and Jean-Paul Guillet[a]

[a] IMS Laboratory, University of Bordeaux, UMR 5218, 351 cours de la Libération 33405 Talence, France.
[b] XLIM Research Institute, UMR 7252 CNRS / University of Limoges, 123 av. A. Thomas 87060, Limoges, France

Corresponding author: jean-paul.guillet@u-bordeaux.fr

***Abstract*—Developments towards the implementation of terahertz pulses imaging system within a guided reflectometry configuration are reported. Two photoconductive antennas patterned on the same LT-GaAs active layer in association with a silica pipe hollow-core waveguide allowed to obtain a guided optics-free imager. Besides working in a pulsed regime, the setup does not require additional optics to focus and couple the terahertz pulses into the waveguide core, simplifying the global implementation in comparison to other reported guided terahertz reflectometry systems. The system is qualified for imaging purposes by means of a 1951 USAF resolution test chart. An image resolution, after a 53 mm propagation length, by about 0.707 LP/mm over the 400-550 GHz integrated frequency band was obtained providing promising basis to pursue the effort towards compact guided pulse imagers for sample inspection within the terahertz range.**

***Index Terms*— Terahertz waveguide, Terahertz transceiver, guided terahertz pulse reflectometry, guided waves, anti-resonant reflections, hollow waveguide, double photoconductive antenna, reflection imaging**

1. INTRODUCTION

The terahertz frequency region has been attracting an increasing amount of attention over the past decades owing to the abilities of these waves to deeply penetrate opaque structures [1] and to identify specific materials through their spectral features. Relevant technologies such as time-domain spectroscopy (TDS) and THz imaging have been used for various applications [2], *e.g.*, analysis of chemical materials [3], metamaterials [4], biomedical [5], non-destructive testing of composite materials [6][7], art painting [8] or electronics packages [9]. Depending on sample properties, terahertz measurements can be performed either in transmission or in reflection mode. However, the transmitted signal may be too low to be detected for absorbing or thick materials. In this case, a THz system in reflection–mode is imperative. Nonetheless, conventional THz sensing systems, using quasi-optic components, only allow to sense along the optical axis dictated by the optics. Besides, the use of optics require specific longitudinal operating distance, alignment and minimum volume for implementation. These reflection modalities are not suitable for applications aiming to probe samples directly *in-situ*, where the energy dissipation within the whole object cannot be ignored.

To overcome these issues, the use of a waveguide as a single-channel medium both to guide the THz pulse directly to the region of interest and to carry the reflected signal seems to be one solution. Such setups are referred as guided terahertz reflectometry (GTR) systems. Even though efficient waveguides to forward terahertz waves are yet to be defined, ideal guiding structures should meet specific requirements: first, low-losses; second, low-dispersion; last, broad frequency bandwidth [10][11]. Throughout the literature, guided reflectometry operations have been realized with different metallic waveguides including metal wire [12] [13] and parallel-plate waveguides (PPWG). Their low dispersion properties in the terahertz regime allow the transmission for a pulse signal. Metal wires have been successfully implemented in

terahertz endoscopic system to probe the bottom of a container [14]. However, this kind of waveguide suffers from poor coupling efficiency and high bending losses which drastically lessens the power of the transmitted signal. On their part, the fundamental propagation mode of PPWGs can be easily excited with a linear polarization. It has been reported that tapered waveguides could resolve features as small as 100 µm [15]. Nevertheless, the difficulty to maintain the structure remains problematic. Apart from metallic waveguides, the dielectric hollow-core waveguides have been tested as alternative components to develop guided terahertz reflectometry systems. Either a lens or a parabolic mirror is included in the system setup to efficiently couple the terahertz signal into the waveguide. They have been used to analyze surface state of objects, to determine molecular concentration and for chemical reaction monitoring [16]. A single–channel flexible waveguide-based terahertz endoscopic system has been demonstrated in 2014 for future clinical application [17]. However, working with optics limits the compactness of such setups. On another hand, dielectric waveguides are commonly employed in association with continuous sources but guided pulsed terahertz reflectometry has yet to be investigated.

Here, we report on further developments towards a reflection-mode setup using a double-PCA transceiver in combination with a hollow-core waveguide. We used the TeraSpike TD-800-TR.5 (*Protemics GmbH* Ltd [18]) to generate and to detect the terahertz pulses. Compared to two independent devices each for generation or detection, this transceiver probe including two PCAs mounted on the same low-temperature growth gallium arsenide (LT-GaAs) is easier to be implemented. Since the LT-GaAs layer carrying two PCAs is deposited at the apex of a slim cantilever (0.18 mm thick and 2 mm wide), the coupling between the transceiver and the waveguide can be achieved without supplemental optics by choosing a suitable waveguide with comparable dimensions. For this reason, a 3 mm diameter hollow-core waveguide was chosen to enable single-channel communication between the transceiver and a sample. The guidance of the waveguide allows to probe the sample in close proximity, to perform measurements both through a slight aperture and *in-situ* over a large frequency bandwidth.

Firstly, the THz transceiver is characterized to assess its intrinsic properties. The radiation pattern of one of the photoconductive antennas (PCA) is computed by means of a 3D electromagnetic (EM) simulator. In parallel, the silica hollow-core waveguide is tested to determine its working spectral band. Following these investigations, the waveguide is implemented in association with the transceiver to build a guided terahertz pulse reflectometry system. Setup performances for imaging purposes are qualified by imaging a 1951 USAF test target.

2. SETUP

2.1. Implementation

As depicted in Figure 1.(a), our GTPR system is similar to a TDS setup. Aside from the terahertz transceiver and the waveguide, the system includes some dedicated optics, a mechanical chopper, a lock-in amplifier and delay line. In combination to the photoconductive receiver on the transceiver, the waveform of terahertz time signal can be retrieved. While an 800 nm wavelength pump beam excites the emitter from the antenna front side, a probe beam, with similar characteristic, illuminates the transceiver detector from the back side. When stimulated by the pump laser, photocarriers are generated within the active layer of the photoconductive material. Those carriers are accelerated by an external bias field and thus drive the patterned antenna [19]. Ultimately, the photocurrent is re-emitted as a terahertz pulse. Thanks to adapted dimensions, the terahertz pulses are then injected into the hollow-core waveguide without help of any optics (Figure 1.(b)). Then, the terahertz signal propagates out of the waveguide and interact with the sample. A fraction of the emitted signal is reflected back to the waveguide's input facet and reach the detector on the transceiver probe. Pulses detection is achieved in an analogous way than their emission. The intensity of the induced photocurrent is proportional to the terahertz field that carries the intrinsic dielectric properties of the sample.

2.2. *Transceiver*

The two photoconductive antennas are patterned on the same LT-GaAs photoconductive layer, whose thickness is by about 1.30 µm. This LT-GaAs layer is located on the apex of a 180 µm thick flexible polyethylene terephthalate (PET) cantilever. Unlike conventional photoconductive antennas using silicon lens to focus and to collect terahertz pulses, the employed device exploits planar quasi-Yagi antennas to radiate and to receive electromagnetic waves. Owning to its great directivity, the use of Yagi antenna has extended from radio frequency domain to higher frequency band, up to the optical region.

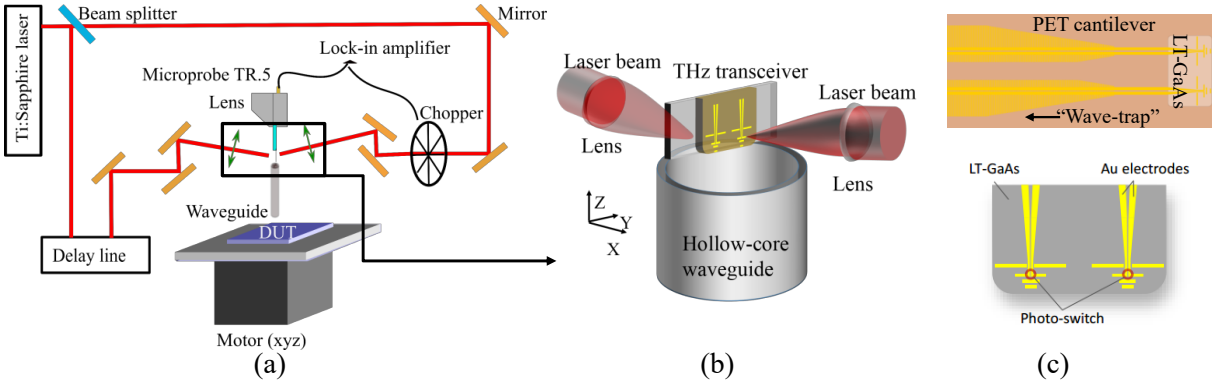

Figure 1: Description of guided terahertz waves reflectometry system setup. (a) Global view of the experimental setup, which is equivalent to a standard TDS system, but with the difference that two focused laser beams are injected on a single chip containing two antennas. The generated wave is then transmitted via the waveguide to the device under test (DUT) and then one fraction of the incident signal comes back through the same waveguide to the other PC antenna acting as detector. (b) Close-up view between the double photoconductive antennas and the waveguide. Back face illumination was preferred for one of PC antennas to avoid congestion issues from the lenses. Since the LT-GaAs layer dimensions are comparable to the diameter of waveguide core, the generated signal is expected to be directly coupled into the waveguide. (c) On the top, schematic view of the PET cantilever. The "wave-trap" design along the two electrode lines is supposed to avoid the overlap of reflections from the sample and probe itself. On the bottom, close-up view of the transceiver probe-tip. Two photoconductive switches with Yagi-Uda antennas are deposited on the LT-GaAs layer.

Terahertz Yagi-Uda antennas depicted in Figure 1.(c) consist of a driven dipole close to the photoconductive switch, a reflector in the rear and two resonators in front. The radiation pattern of the antennas has been evaluated by a 3D electromagnetic simulator (CST Microwave Studio®) and 2D polar diagrams are depicted in Figure 2.

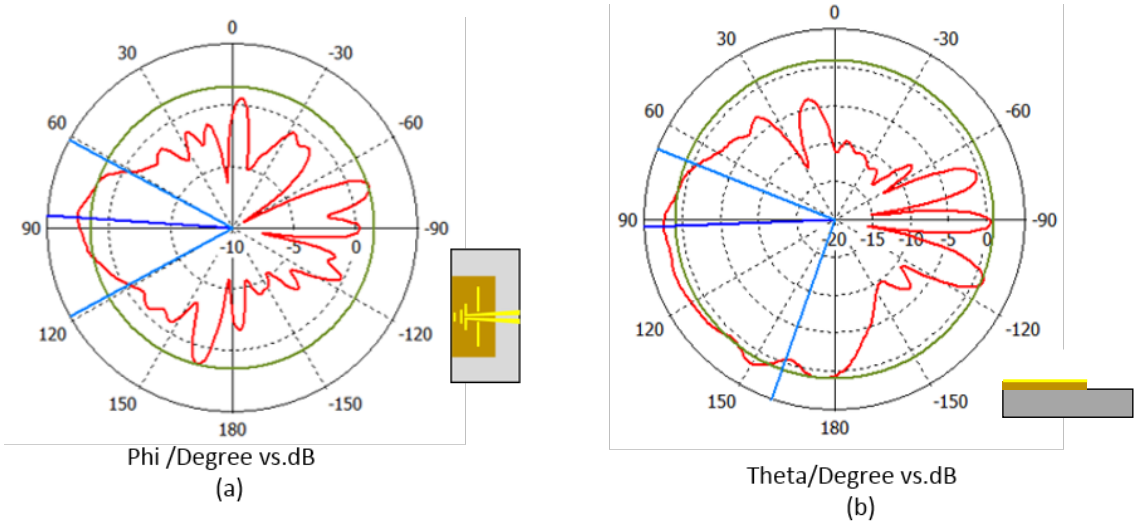

Figure 2: 2D radiation pattern at 400 GHz, calculated by the EM simulator CST. (a) Directivity of antenna when theta = 90° (E-plane). Phi = 86° is the main lobe direction, towards the front of antenna. (b) Directivity of antenna when phi = 90° (H-plane). Theta = 92° is the main lobe direction, towards the front of antenna. Besides, we can observe that the radiated wave is more toward the substrate.

The E-plane exhibits a main lobe (Phi = 86°) oriented in the direction of the antenna, which corresponds to the typical response of the Yagi-Uda antenna [20]. Impacted by the high refractive index of the substrate, the generated waves tend to radiate into free space toward the substrate, which was demonstrated in the polar diagram along H-plane (shown in Figure 2.(b)). Besides, back lobe in the radiation pattern reveals that an important fraction of generated signal propagates towards the transceiver base. It may produce some unwanted echoes from the transceiver base back to the PCA. Thus, perpendicular lines, called *wave-traps* are patterned on the transceiver metallic lines to reduce the internal reflections and hence to avoid the superposition of reflected signals from the two opposite directions [21]. In the case that two PCAs are presented on the LT-GaAs layer, their side lobes (shown in the radiation pattern along the E-plane) lead to a direct communication between them. In order not to assign this direct transmission as a result of the interaction between the emitted radiations and the sample, a metal sheet acting as a perfect mirror was placed directly below the transceiver with varying distance of 2 mm (shown in Figure 3.(a)). Two contributors have then been recorded: first, the signal arising from the direct transmission between the two antennas; second, the reflections occurring at the metallic plate surface. While the first contribution, attributed to the cross talking effect, remains consistent for different mirror distances, signals due to the reflection from the metallic plate obviously exhibit time delay and amplitude decrease with increasing distances. In addition, compared with the direct transmitted signal between two PCAs whose spectral width extends from 200 GHz to 1.2 THz, reflections from the metallic surface present a useful bandwidth up to 700 GHz mainly limited by the low total radiation efficiency of the antenna at high frequency (shown in Figure 3.(b)).

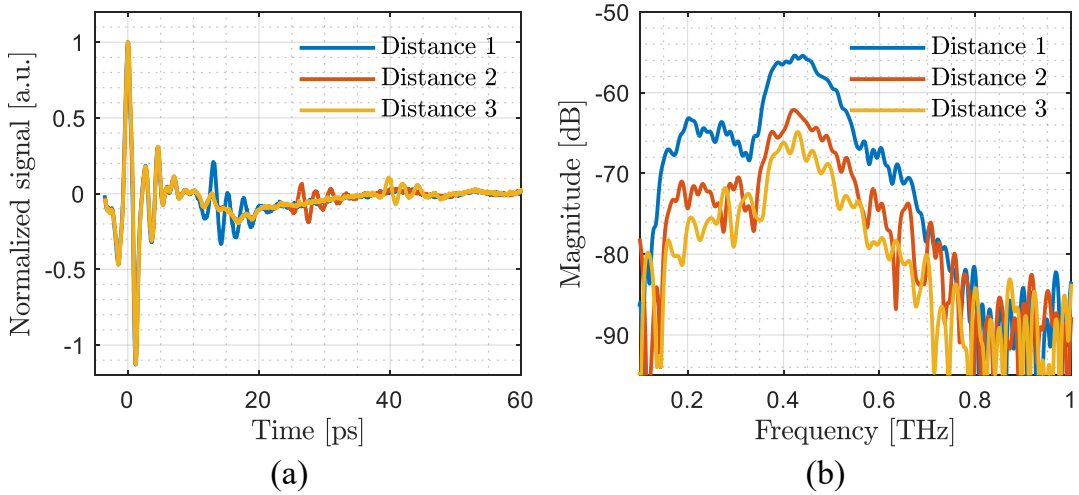

Figure 3: Detected signals with different distances between the transceiver and metal sheet (2-mm-step). (a) Time domain signal. There is an overlapped part among different measurements (for example, when t = [0-10] ps), which corresponds to a reference signal obtained by the cross-talking between the emitter and the detector. (b) Spectrum of the signal reflected by the metal in a varying distance. As the propagation distance increases, reflections become weaker. The transceiver has successfully detected these reflections, and it is more sensitive to the frequencies between 200 GHz and 700 GHz.

2.3. Hollow-core waveguide

Since the distance between the two photoconductive antennas is around 700 µm, the waveguide to be implemented within a guided pulse terahertz reflectometry system has to have a comparable diameter size to realize an optics-free single channel communication. Dielectric hollow-core waveguides exploits the anti-resonant effect as a guiding mechanism. The high-index cladding layer acts as a Fabry-Pérot cavity while the low-index core allows the terahertz wave propagation at non-characteristic frequencies. The characteristic frequencies of the cladding are defined by [22][23]:

$$f_m = \frac{mc}{2t\sqrt{n^2-1}} \quad (1)$$

where c is the speed of the light in vacuum, m is an integer, t and n are the thickness and refractive index of the cladding respectively. Low-loss propagations within the waveguide are expected owing to the low absorption of terahertz frequencies in air core of the waveguide. In view of the foregoing, a silica pipe hollow-core waveguide with a diameter of 3 mm and a thickness of 130 µm has been chosen. In such a selected case, t = 130 µm and n = 1.97. Characteristic frequencies of the silica cladding are expected to be around 687 GHz, 1.37 THz and 2.06 THz. By using a fiber TDS system (TPS4000, TeraView Ltd., Cambridge UK), two waveguides with different lengths (201 and 301 mm respectively) have been characterized in transmission-mode configuration. Since the incident beam size from the terahertz source is bigger than the dimension of the waveguide, a polyethylene lens is inserted between the emitter and the waveguide to facilitate the coupling. As indicated in Figure 4, the dips in the spectrum of the transmitted signal correspond appropriately to calculated resonant frequencies, confirming the waveguide's guiding mechanism. Moreover, the exhibited waveguide behavior reports relatively large carrying bandwidth from 350 GHz up to 650 GHz. As consequence, such a guiding structure is matching supported frequency band, enabling a simple coupling setup and low dielectric loss expectations [24].

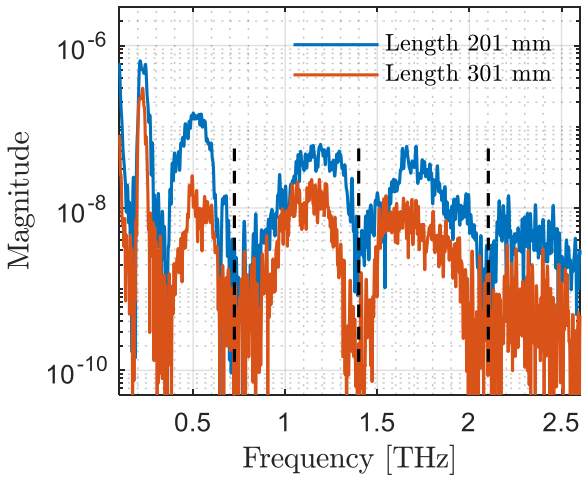

Figure 4: Spectrum of the transmitted signals via silica hollow-core waveguides with different lengths. (Blue curve: 201 mm length waveguide. Red curve: 301 mm length waveguide.) The expected resonant frequencies of silica cladding (f = 687 GHz, 1.37 Terahertz and 2.06 Terahertz) are marked with the vertical dash-dot lines. The corresponding attenuation peaks in the spectrum demonstrate that this waveguide exploit the antiresonant reflections as guiding mechanism.

2.4. Full setup 3D simulation

In order to estimate the portion of energy transferred from the terahertz transceiver to the waveguide core, a FDTD simulation was performed. The energy density was successively calculated at two distinct sections: first, the surface directly subsequent to the end of the transceiver (S_1); second, the interface section between free space and the waveguide, located 900 µm from the transceiver (S_2). The energy density transfer between the transceiver to the waveguide was then determined as:

$$\eta(f) = \frac{\oiint_{S_2} \frac{1}{2}\varepsilon_0\varepsilon_r |E_{in}(x,y,z)|^2 dxdy}{\oiint_{S_1} \frac{1}{2}\varepsilon_0\varepsilon_r |E_{out}(x,y,z)|^2 dxdy} \quad (2)$$

where S_1 and S_2 are the respective sections onto which are summed the energy fractions and where E_{in} and E_{out} stand for the energy entering the waveguide and emitted by the transceiver, respectively. The energy density coupled to the waveguide as a function of the frequency is depicted in Figure 5. The maximum

transfer has been found at 340 GHz with an efficiency by about 22.78 % while the lowest transfer is located at 490 GHz with a respective efficiency of 13.25 %. Further simulations were performed to assess the propagation of the terahertz pulses along the waveguide. To this aim, a metal plate was numerically placed at the end of the waveguide to maximize the back end reflection, which is not displayed in the simulation model given in Figure 6.(a) . The absolute value of the electric field at various propagation time is shown in Figure 6.(b). At t = 10 ps the wave appears at the photoconductive antenna emitter, then propagates to the end of the waveguide. Figure 6.(c) displays the signal measured at the second antenna port. From 0 ps to 25 ps, the recorded signal corresponds to the direct communication between the two antennas. From 25 ps to 50 ps the signal corresponds to the reflected portion at the entrance of the hollow-core waveguide. The signal reflected from the back end is recorded from t = 360 ps. Finally, on Figure 6.(d) a focus is given on the reflected signal, which consists of several main oscillations and of higher modes propagating more slowly in the high-index cladding layer.

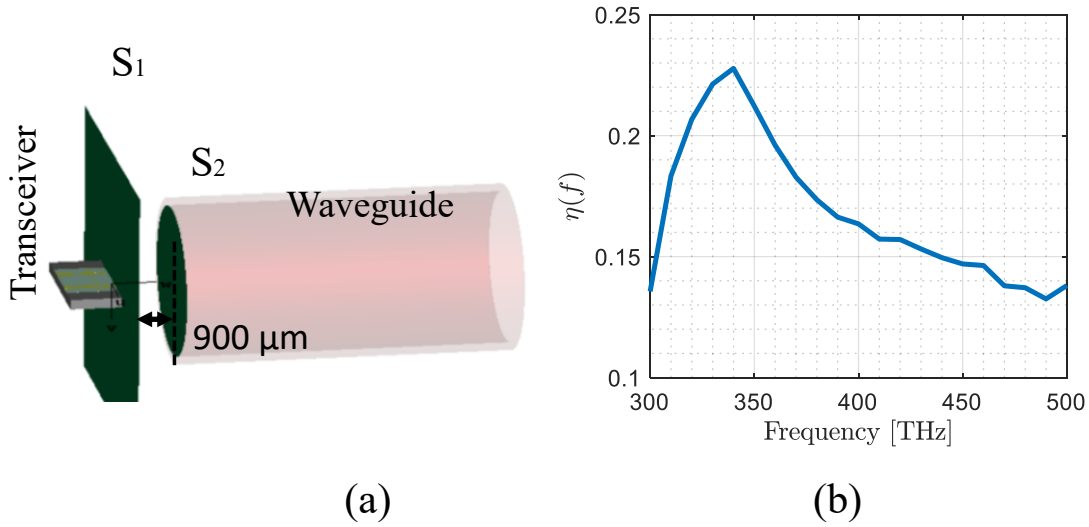

Figure 5: (a) Model of the transceiver probe and hollow-core waveguide in CST. The distance between the transceiver probe tip and the waveguide is 900 µm. While the first rectangle section is placed at the probe tip of the transceiver to calculate the radiated energy by the transceiver, the second circle section lies at the input facet of the waveguide to evaluate the received energy. (b) By comparing the energy passing through two sections, the portion directly injected into the waveguide can be obtained.

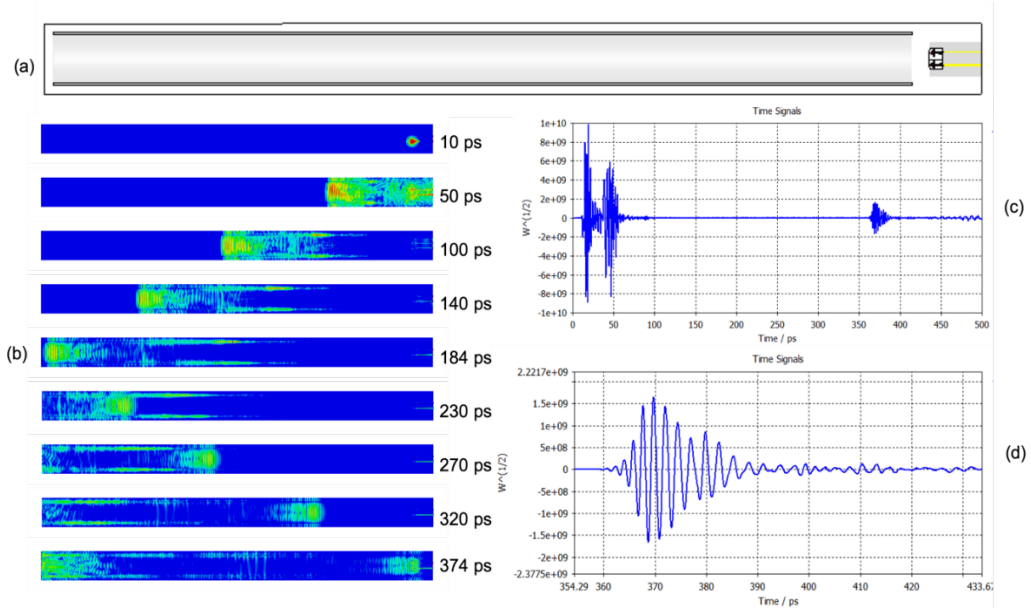

Figure 6: Full simulation of the setup (a) Scheme of the model (b) Cross-section along the waveguide of the absolute value of the electric field at different time of simulation. (c) Reflected signal obtained at the detector PCA port (d) Zoom on the signal correspond on the reflection at the end of the waveguide.

3. EXPERIMENTAL RESULTS

3.1. Time domain result

The benefits of wave guiding lie in the fact that terahertz waves can reach farther targeted site of inspection while minimizing energy dissipation in comparison to free space propagation. This aspect was verified by measuring the reflected signal from a metal plate situated 53 mm from the terahertz transceiver (just below the waveguide's output). The reflected signal was hence compared between free space propagation to that of guided regime. Results are reported in Figure 7, including originally detected signals (a) and reflected signals from sample (b) after removing the direct transmission signal between two PCAs.

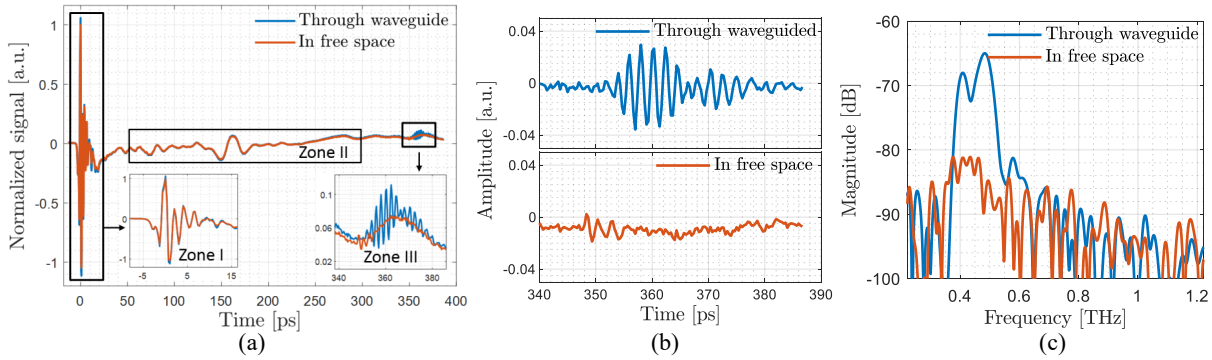

Figure 7: (a) Detected signals by the Terahertz transceiver. Blue curve: signal propagating through the waveguide. Red curve: signal propagating in air (baseline). We divided this signal into three zones. First, the zone I (t = [0-30] ps) corresponds to the cross-talking between the two photoconductive antennas, it can be obtained even without the sample. Then the zone II (t=[30 -250] ps) corresponds to reflection signal coming from probe-mount and imperfection of wave trapping design [16]. Finally, in the zone III (after 340 ps) we observe the reflected signal from the sample at the end of the waveguide (blue curve) and a weak reflected signal by freely propagation (red curve). (b) Pure reflections from metal in the time domain. (c) Spectrum of reflection signals obtained at Figure 7. (b). It demonstrates that more signal power is transmitted compared to freely propagation owning to the guidance of glass waveguide.

As expected from a guiding structure, guided terahertz pulses exhibit a significantly higher amplitude compared to that of non-guided ones. The power fraction carried by reflected pulses propagating through the hollow-core waveguide is roughly 12 dB greater than that of those propagating in free space for

frequencies spanning from 400 to 650 GHz (shown in Figure 7.(c)). Such a working frequency band is mainly determined by both the terahertz transceiver response and the waveguide propagation modes. Nevertheless, the reflected signal propagating through the waveguide are impacted by signal distortions in the time-domain.

3.2. Imaging results

After the demonstration of an effective terahertz pulse guidance, we focus on the reflection imaging capabilities of this system. As represented in Figure 8. (a), a positive 1951 USAF resolution test target is placed just below the output of waveguide (a distance less than 0.5 mm). The scanned zones cover elements in group -1 and -2, which are mentioned with red rectangles. By moving the 1951 USAF test chart, a raster scan is performed to record time signal at each point. A pixelated data map is eventually constructed. An image can be obtained both in time or frequency domain by different mathematical criteria [25]. For example, by integrating frequency components from 400 GHz to 550 GHz, two images have been extracted (Figure 8.(b) and (c)). Line profiles of terahertz magnitude along the solid line AB in group -2 and line A'B' in group -1 are additionally provided. The resolution is given in pairs of lines (a transparent and a reflective) per millimeter (pl/mm) or in thickness of the corresponding line. When the contrast between bars and substrate is lower than 0.3 it is estimated that two stripes cannot be differentiated. Therefore, lines are still clearly distinguished until the element 4 in group -1. The width of line is about 707 µm and the spatial frequency is about 0.707 LP/mm. The imaging performance is mainly limited by the non-perfect frequency match between the transceiver and the waveguide, the laser noise and the mechanical constraints of motorized stage.

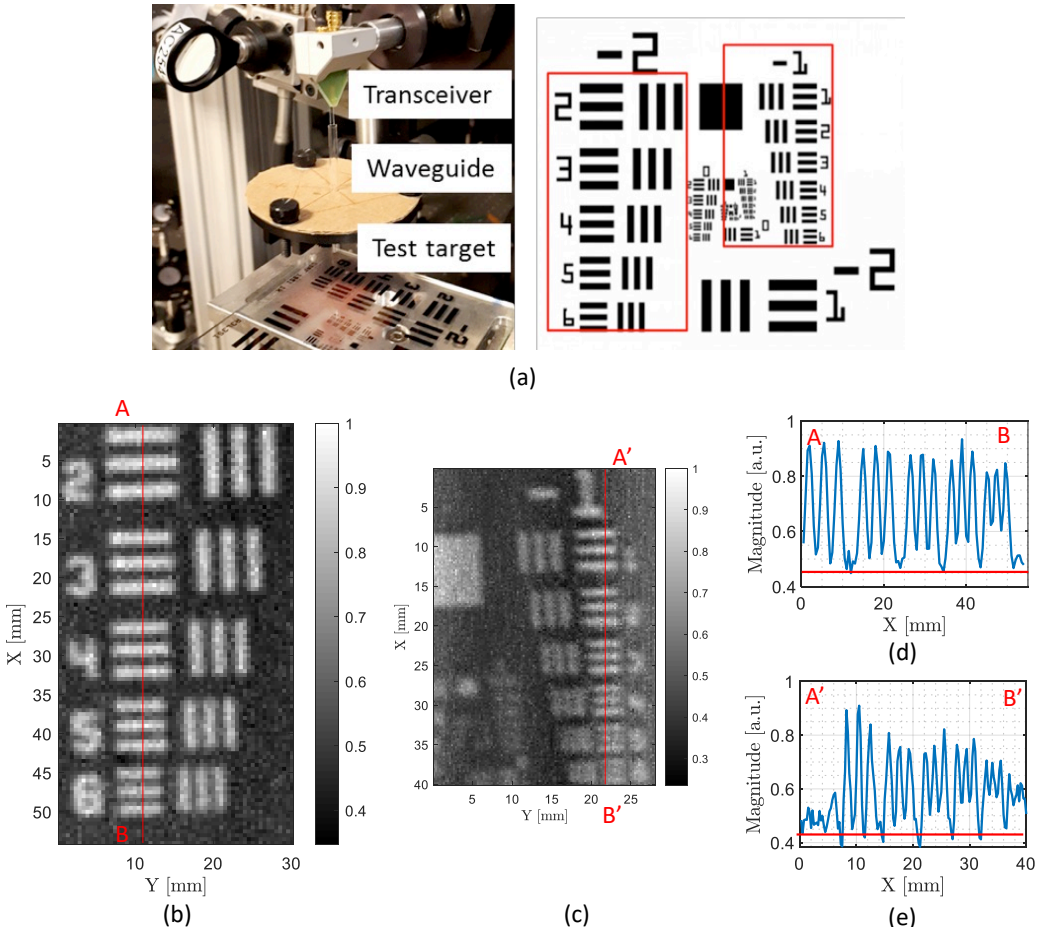

Figure 8: (a) Left: Photography of experimental setup. The silica hollow-core waveguide is placed below the terahertz transceiver and a 1951 USAF test target as sample is mounted on the linear translation stages. Right: 1951 USAF test target image, in which the scanned areas are marked by the red rectangles. (b) and (c) Two images of the scanned areas (elements in group -1 and in group -2 respectively) are obtained from

the trapezoidal integration between 400 and 550 GHz. (d) and (e) The line profiles of terahertz field magnitude along the solid line AB in group -2 and solid line A'B' in group -1.

4. CONCLUSION

In this work, a guided terahertz pulse reflectometry system has been successfully constructed by taking advantage of a terahertz waveguide and a transceiver. The generation and detection of terahertz radiations are realized by using a terahertz transceiver while terahertz waves are guided by a waveguide. Silicon lens, beam splitter or coupler is no more required to manipulate the terahertz beam in free space, which makes this system setup more compact and easier to align. In the future, an integrated system with antenna and a waveguide could be convenient for terahertz imaging experiment having spatial issues.

ACKNOWLEDGMENT

This work was supported in part by the French Ministry of National Education, Research and Technology.

REFERENCES

[1] D. M. Sheen, D. L. McMakin, and T. E. Hall, "Three-dimensional millimeter-wave imaging for concealed weapon detection," *IEEE Trans. Microw. Theory Tech.*, vol. 49, no. 9, pp. 1581–1592, 2001.

[2] S. S. Dhillon, M. S. Vitiello, E. H. Linfield, and E. Al, "The 2017 terahertz science and technology roadmap," *J. Phys. D. Appl. Phys.*, vol. 50, p. 43001, Feb. 2017.

[3] J. A. Zeitler, P. F. Taday, D. A. Newnham, M. Pepper, K. C. Gordon, and T. Rades, "Terahertz pulsed spectroscopy and imaging in the pharmaceutical setting - a review," *J. Pharm. Pharmacol.*, vol. 59, no. 2, pp. 209–223, 2007.

[4] O. Mitrofanov, F. Dominec, P. Kužel, J. L. Reno, I. Brener, U.-C. Chung, C. Elissalde, M. Maglione, and P. Mounaix, "Near-field probing of Mie resonances in single TiO 2 microspheres at terahertz frequencies," *Opt. Express*, vol. 22, no. 19, pp. 23034–23042, 2014.

[5] U. R. Pfeiffer, P. Hillger, R. Jain, J. Grzyb, T. Bücher, Q. Cassar, G. MacGrogan, J.-P. Guillet, P. Mounaix, and T. Zimmer, "Ex Vivo Breast Tumor," *IEEE Microw. Mag.*, vol. 20, no. 9, pp. 32–46, 2019.

[6] Q. Cassar, A. Chopard, F. Fauquet, J.-P. Guillet, M. Pan, J.-B. Perraud, and P. Mounaix, "Iterative Tree Algorithm to Evaluate Terahertz Signal Contribution of Specific Optical Paths within Multi-Layered Materials," *IEEE Trans. Terahertz Sci. Technol.*, 2019.

[7] F. Friederich, K. May, B. Baccouche, C. Matheis, M. Bauer, J. Jonuscheit, M. Moor, D. Denman, J. Bramble, and N. Savage, "Terahertz Radome Inspection," *Photonics*, vol. 5, no. 1, p. 1, 2018.

[8] C. L. K. Dandolo, J.-P. Guillet, X. Ma, F. Fauquet, M. Roux, and P. Mounaix, "Terahertz frequency modulated continuous wave imaging advanced data processing for art painting analysis," *Opt. Express*, vol. 26, no. 5, p. 5358, 2018.

[9] E. Kowalczuk, A. Bhattacharya, K. C. Lee, E. Alton, J. Alton, M. Igarashi, and S. Barbeau, "Fault localisation of defects using electro optical terahertz pulse reflectometry and 3D em modelling with virtual known good device," in *2014 International 3D Systems Integration Conference, 3DIC 2014 - Proceedings*, 2014, pp. 1–4.

[10] D. A. Shaghik Atakaramians, Shahraam Afshar V., Tanya M. Monro, "Terahertz dielectric waveguides," *Adv. Opt. Photonics*, vol. 6, pp. 293–339, 2014.

[11] H. Bao, K. Nielsen, O. Bang, and P. U. Jepsen, "Dielectric tube waveguides with absorptive cladding for broadband, low-dispersion and low loss THz guiding," *Sci. Rep.*, vol. 5, 2015.

[12] J. P. Guillet, L. Chusseau, R. Adam, T. Grosjean, A. Penarier, F. Baida, and D. Charraut, "Continuous-wave scanning terahertz near-field microscope," *Microw. Opt. Technol. Lett.*, vol. 53, no. 3, pp. 580–582, 2011.

[13] L. Chusseau and J.-P. Guillet, "Coupling and propagation of Sommerfeld waves at 100 and 300 GHz," *J. Infrared, Millimeter, Terahertz Waves*, vol. 33, no. 2, pp. 174–182, 2012.

[14] K. Wang and D. M. Mittleman, "Metal wires for terahertz wave guiding," *Nature*, vol. 432, no. 7015,

pp. 376–379, 2004.
[15] M. Awad, M. Nagel, and H. Kurz, “Tapered Sommerfeld wire terahertz near-field imaging,” *Appl. Phys. Lett.*, vol. 94, no. 5, pp. 3–6, 2009.
[16] B. You and J.-Y. Lu, “Remote and in situ sensing products in chemical reaction using a flexible terahertz pipe waveguide,” *Opt. Express*, vol. 24, no. 16, p. 18013, 2016.
[17] P. Doradla, K. Alavi, C. Joseph, and R. Giles, “Single-channel prototype terahertz endoscopic system,” *J. Biomed. Opt.*, vol. 19, no. 8, 2014.
[18] Protemics, “TeraSpike TD-800-TR.5.”Available: http://www.protemics.com/index.php/products/teraspike/td-800-tr.
[19] E. Castro-Camus and M. Alfaro, “Photoconductive devices for terahertz pulsed spectroscopy,” *Photonics Res.*, vol. 4, no. 3, p. A36, 2016.
[20] H. Yagi and S. Uda, “Projector of the Sharpest Beam of Electric Waves,” in *Proceedings of the Imperial Academy*, 1926, vol. 2, no. 2, pp. 49–52.
[21] B. Guo, “Revealing the Truth About ‘ Trapped Rainbow ’ Storage of Terahertz Waves in Plasmonic Grating,” *Plasmonics*, pp. 1–6, 2017.
[22] C. Lai, B. You, J. Lu, T. Liu, J. Peng, C. Sun, and H. Chang, “Modal characteristics of antiresonant reflecting pipe waveguides for terahertz waveguiding,” *Opt. Express*, vol. 18, no. 1, p. 309, 2010.
[23] E. Nguema, D. Férachou, G. Humbert, J. Auguste, and J. Blondy, “Broadband terahertz transmission within the air channel of thin-wall pipe,” *Opt. Lett.*, vol. 36, no. 10, pp. 1782–1784, 2011.
[24] J.-Y. Lu, C.-P. Yu, H.-C. Chang, H.-W. Chen, Y.-T. Li, C.-L. Pan, and C.-K. Sun, “Terahertz air-core microstructure fiber,” *Appl. Phys. Lett.*, vol. 92, no. 6, p. 064105, 2008.
[25] H. Balacey, B. Recur, J.-B. Perraud, J. B. Sleiman, and P. Mounaix, “Advanced Processing Sequence for 3-D THz Imaging,” *IEEE Trans. Terahertz Sci. Technol.*, vol. 6, no. 2, pp. 191–198, 2016.